Available online at website: https://journal.bcrec.id/index.php/bcrec

Bulletin of Chemical Reaction Engineering & Catalysis, 19 (2) 2024, 361-371

Research Article

Performance of Hydrothermally Prepared NiMo Dispersed on Sulfated Zirconia Nano-catalyst in the Conversion of Used Palm Cooking Oil into Jet Fuel Range Bio-hydrocarbons

Karna Wijaya[1], Aldino Javier Saviola[1,*], Amalia Kurnia Amin[2], Marini Fairuz Vebryana[1], Adyatma Bhagaskara[1], Hilda Anggita Ekawati[1], Saffana Ramadhani[1], Dita Adi Saputra[3], Agustanhakri Agustanhakri[3]

[1]Department of Chemistry, Faculty of Mathematics and Natural Sciences, Universitas Gadjah Mada, Yogyakarta 55281, Indonesia.
[2]Research Center for Chemistry, National Research and Innovation Agency (BRIN), The B. J. Habibie Science and Technology Area, South Tangerang, Banten 15314, Indonesia.
[3]Research Center for Energy Conversion and Conservation, National Research and Innovation Agency (BRIN), The B. J. Habibie Science and Technology Area, South Tangerang, Banten 15314, Indonesia.

Received: Received: 9th May 2024; Revised: 8th July 2024; Accepted: 8th July 2024
Available online: 15th July 2024; Published regularly: August 2024

Abstract

Human efforts to overcome environmental problems from using fossil fuels continue, such as hydroconversion of biomass into bio-jet fuel. Research on producing a jet fuel range of bio-hydrocarbons from used palm cooking oil catalyzed by sulfated zirconia impregnated with nickel-molybdenum bimetal has been successfully conducted. The hydrothermal method synthesized the nano-catalyst material in the sulfation and impregnation processes. The hydroconversion process was carried out at atmospheric pressure and a temperature of 300–600 °C for 2 h with a hydrogen gas flow rate of 20 mL/min and a catalyst-to-feed ratio of 1:100 (wt%). Compared with zirconia and sulfated zirconia, NiMo-impregnated sulfated zirconia showed the best activity and selectivity in bio-jet fuel production with liquid product and selectivity of 61.07% and 43.49%, respectively. This catalyst also performed well in three consecutive runs, with bio-jet fuel selectivity in the second and third runs of 51.68% and 30.86%, respectively.

Keywords: Bio-jet fuel; NiMo/sulfated zirconia; used palm cooking oil; hydroconversion

How to Cite: K. Wijaya, A.J. Saviola, A.K. Amin, M.F. Vebryana, A. Bhagaskara, H.A. Ekawati, S. Ramadhani, D.A. Saputra, A. Agustanhakri (2024). Performance of Hydrothermally Prepared NiMo Dispersed on Sulfated Zirconia Nano-catalyst in the Conversion of Used Palm Cooking Oil into Jet Fuel Range Bio-hydrocarbons. *Bulletin of Chemical Reaction Engineering & Catalysis*, 19 (2), 361-371 (doi: 10.9767/bcrec.20157)

Permalink/DOI: https://doi.org/10.9767/bcrec.20157

1. Introduction

Fossil fuels are the heart of global transportation energy sources, making up the world's largest and most used energy source. Jet fuel, also known as aviation turbine (avtur) fuel, is a fossil fuel derivative for powering up aircraft turbine engines. The use of this fuel has increased with the high demand for flight in all countries worldwide. Jet fuels from fossil fuels produce greenhouse gases, especially NO_x and CO_2 gasses, accounting for 13.3% of all mobile transportation [1]. This trend is projected to increase rapidly to 3100 million tons of CO_2 gas emission in 2050 [2]. These problems attracted researchers' awareness of the need to develop greener fuels from biomass, such as bio-jet fuel. Using bio-jet fuel can reduce greenhouse gas emissions because it is produced by plants that adsorb CO_2, thus creating a carbon recycling cycle [3]. Using bio-jet fuel also does not require engine system modification in aircraft [4].

Palm oil is a vegetable oil that can be used to fry food. Palm oil's physical and chemical changes after prolonged cooking may cause many serious

* Corresponding Author.
Email: aldino.javier@mail.ugm.ac.id (A.J. Saviola)

health hazards. Used palm cooking oil also causes serious environmental problems. It can cause a foul odor and pollute water if poured into natural water [5]. To address these problems, the hydroconversion of used palm cooking oil to produce bio-jet fuel is a great innovation. Vegetable oil contains triglycerides and free fatty acids that can be converted to hydrocarbon compounds in jet fuel fraction (C_8–C_{16}). The catalytic conversion of triglycerides into hydrocarbons occurs through three reactions of hydroconversion, which are hydrodeoxygenation (HDO), decarbonylation (DCO), and decarboxylation (DCO_2) [6]. Even-numbered alkanes are produced via hydrodeoxygenation, while decarboxylation and decarbonylation processes produce odd-numbered alkanes. Hydrocracking and hydroisomerization change the lengthy chain of typical alkanes into a straight and branched chain alkane [7].

The development of heterogeneous catalysts for biofuel production is highly impactful due to their advantages of easy separation, advanced selectivity, and reuse capability. Zirconia (ZrO_2) has garnered significant interest in catalytic reactions because it has high thermal stability, excellent ionic conductivity, and low thermal conduction, making it preferable as a support material for catalysts [8−11]. The acidity of ZrO_2 can be enhanced by coating the surface with an acid solution, such as H_2SO_4, to create sulfated zirconia. However, using sulfated zirconia as a catalyst for hydroconversion still has the disadvantage of deactivation due to coke buildup, even though this material has shown good acidity.

Further catalyst modification to improve catalytic processes is mainly done by incorporating transition metals, such as Pt, Pd, Co, Cr, Ni, and Mo [12,13]. Nickel and molybdenum emerge as competitive and efficient catalysts for bio-jet fuel production compared to other transition metals due to their advantageous reactivity and stability throughout the conversion processes [11,14]. Utilizing nickel-based catalysts, typically supported on zeolites, has demonstrated notable efficacy and stability in bio-jet fuel production [15]. Likewise, molybdenum has proven effective in the hydroconversion process of palm oil into bio-jet fuel, showcasing its potential to yield bio-jet fuel with desirable properties [16]. The presence of nickel and molybdenum metals within the catalyst framework induces a synergistic effect. Both metals nearby facilitate interactions and cooperative impact, increasing catalytic activity compared to the individual metals alone [17,18]. Nickel excels at catalyzing the breakdown of organic molecules into light-chain hydrocarbons [19], and molybdenum specializes in hydrodeoxygenation, resulting in a more selective yield during hydroconversion [20].

This research aims to synthesize NiMo bimetal supported on sulfated zirconia catalysts via a hydrothermal method, assessing their efficacy in bio-jet fuel production. While prior studies have synthesized NiMo-sulfated zirconia catalysts using stirring techniques primarily targeting gasoline production [21], the hydrothermal technique for bio-jet fuel production has yet to be reported. It is well-established that the hydrothermal process makes assessing the effect of various synthesis parameters simple and organized [22]. Additionally, it permits the control of crystal growth, particle size, shape, and several other characteristics [23]. Therefore, the results of this study are expected to provide information on the catalytic ability of hydrothermally synthesized NiMo/sulfated zirconia catalyst in converting used palm cooking oil into bio-jet fuel so that this catalyst can be considered as a candidate for further study on an industrial scale biofuel.

2 Materials and Methods

2.1 Materials

The materials used for catalyst fabrication in this study were commercial nano-zirconia powder (ZrO_2, 99.9%) purchased from Jiaozuo Huasu Chemical Co., Ltd, China; sulfuric acid (H_2SO_4, 98%), nickel salt precursor ($NiCl_2 \cdot 6H_2O$, 99.9%), molybdenum salt precursor ($(NH_4)_6Mo_7O_{24} \cdot 4H_2O$, 99.9%), and pyridine ($C_5H_5N$, 99.9%) were supplied from Merck. The other materials used included deionized water and natural bentonite from CV Fruitanol Energy; nitrogen gas (N_2) and hydrogen gas (H_2) were supplied from PT Surya Indotim Imex. Used palm cooking oil obtained from an eatery in Yogyakarta and commercial jet fuel was obtained from PT Pertamina.

2.2 Sulfated Zirconia (SO_4–ZrO_2) Preparation

A total of 10 g of ZrO_2 powder was placed into an autoclave reactor with 100 mL of H_2SO_4 2 M solution. The mixture was stirred for 30 min and then heated at 120 °C for 5 h. The solids were separated by centrifugation for 20 min at 2000 rpm, and then the solids were dried at 100 °C for 2 h. The dried solid was then calcined at 500 °C for 4 h in a furnace and then crushed and sieved with a 270-mesh sieve to obtain sulfated zirconia (SO_4–ZrO_2).

2.3 Synthesis of NiMo-impregnated Sulfated Zirconia (NiMo/SO_4–ZrO_2)

Nickel and molybdenum bimetal impregnation was carried out by co-impregnation, with the concentration of each metal salt precursor at 1% (wt%) for 5 g of sulfated zirconia. The nickel and molybdenum precursors were first

dissolved in 50 mL of deionized water in an autoclave reactor. Afterward, sulfated zirconia was added to the solution and stirred for 30 min. The mixture was then heated at 120 °C for 5 h. The solution was then evaporated at 100 °C for 4 h. The dried solid was then calcined at 500 °C for 5 h with an N_2 gas flow rate of 20 mL/min and reduced at the same temperature for 5 h with an H_2 gas flow rate of 20 mL/min to obtain NiMo-impregnated sulfated zirconia ($NiMo/SO_4–ZrO_2$).

2.4 Characterization of the Catalysts

The crystallinity study of the catalyst material was carried out using an X-ray Diffractometer (XRD, Brucker D8 Advanced Eco) instrument with Cu-Kα = 1.54060 Å at 2θ of 10–80°. The crystallite size of each sample was determined using the Scherrer equation in Equation (1) by taking the 2θ value for the characteristic peak of monoclinic zirconia with the highest intensity at 28.27°, k = 0.94, λ = 0.1546 nm, and β is Full Width at Half Maximum (FWHM).

$$d = \frac{k\lambda}{\beta \cos\theta} \quad (1)$$

The functional groups on the catalyst material were identified using a Fourier Transform Infrared (FTIR, Shimadzu Prestige-21) spectrometer instrument by KBr pellet technique at a 400–4000 cm^{-1} wavenumber. The Surface Area Analyzer (SAA, Micromeritics Gemini VII Version 5.03) instrument studied each catalyst material's surface area and pore characteristics with a degassing temperature of 300 °C. The morphological structure and elemental content on the surface of catalyst materials were studied using a Scanning Electron Microscope connected to an Electron-Dispersive X-ray (SEM–EDX, JEOL JED-2300) spectrometer instrument.

The total acidity of the catalyst materials was determined using a Temperature-Programmed Desorption of Ammonia (NH_3-TPD, Micromeritrics Chemisorb 2750). After 30 min of NH_3 adsorption (5% in He, v/v) at 100 °C, it was purged with inert He gas at the same temperature for 30 min. Afterward, NH_3 desorption occurred at 100–700 °C at a heating rate of 10 °C min^{-1}. Meanwhile, the surface acidity test of the catalyst materials was carried out using the gravimetric pyridine method, in which the surface acidity value was determined using Equation (2).

$$Surface\ acidity\ (mmol/g) = \frac{w_2 - w_1}{(w_1 - w_0) \times MW\ pyridine} \times 1000 \quad (2)$$

2.5 Hydroconversion of Used Palm Cooking Oil into Jet Fuel Range Bio-hydrocarbons

Before being used as feed, used palm cooking oil was removed from the water content by oven at 120 °C for 2 h and bleached using the adsorption method with natural bentonite as much as 3% (wt%) at 120 °C for 1 h. Hydroconversion of used palm cooking oil was carried out using a semi-batch reactor with a double furnace (top furnace for catalyst, down furnace for feed) with 30 g feed and 0.3 g catalyst and an H_2 gas flow rate of 20 mL/min. The feed vaporization temperature was set from 300–600 °C while the catalyst furnace temperature was set at 200 °C. Hydroconversion was stopped when no more liquid product was dripping at the feed furnace temperature of 600 °C. Liquid products from hydroconversion were characterized by a Gas Chromatography-Mass Spectrometer (GC–MS, Shimadzu QP2010S) instrument with DB-5MS column length of 30 m, ID of 0.25 mm, and film of 0.25 µm. The unreacted feed that is calculated as residue (R) and total conversion of the feed (TC), as well as the hydroconversion products in the form of liquid (L), gas (G), and coke (C) products, are calculated by Equations (3)–(7).

$$R(wt\%) = \frac{R(g)}{F(g)} \times 100\% \quad (3)$$

$$TC(wt\%) = \frac{F(g) - R(g)}{F(g)} \times 100\% \quad (4)$$

$$L(wt\%) = \frac{L(g)}{F(g)} \times 100\% \quad (5)$$

$$C(wt\%) = \frac{C_f(g) - C_i(g)}{F(g)} \times 100\% \quad (6)$$

$$G(wt\%) = \frac{F(g) - L(g) - C(g) - R(g)}{F(g)} \times 100\% \quad (7)$$

where, R is weight of residue, F is weight of feed, L is weight of liquid product, C is weight of coke, C_f is weight of catalyst final, and C_i is weight of catalyst initial. Meanwhile, the selectivity (S) of the catalysts toward the liquid product in several fractions are calculated by Equation (8).

$$S(wt\%) = \frac{GC-MS\ fraction\ area(\%)}{total\ GC-MS\ area} \times L(wt\%) \quad (8)$$

3. Results and Discussion

3.1 The Crystallinity of the Catalysts

Figure 1 presents XRD diffractograms of zirconia, sulfated zirconia, and NiMo-impregnated sulfated zirconia samples. Meanwhile, Table 1 presents each sample's degree of crystallinity and crystallite size values. The crystal phase of zirconia identified for all samples is monoclinic with 2θ at 24.13, 28.27, 31.53, 34.20,

35.37, 38.65, 40.82, 49.32, 50.20° (ICDD 037-1384) [24]. The addition of sulfuric acid to zirconia hydrothermally gave rise to new crystals, namely the hydrated salt $Zr(SO_4)_2 \cdot 4H_2O$ with orthorhombic crystal phase found at diffraction angles of 13.78, 18.34, 20.55, 25.90, and 30.12° (ICDD 08-0495) [25]. The sulfation treatment of zirconia also causes a decrease in the intensity of the monoclinic phase of zirconia, which indicates the closure of the crystalline surface of zirconia by sulfate ions. This phenomenon is further supported by the sulfated zirconia sample's lower degree of crystallinity.

The impregnation of nickel and molybdenum bimetal on sulfated zirconia does not give rise to new peaks in the X-ray diffractogram. This is possible because the concentration of the dispersed metals is too small to disturb the parent crystal of the zirconia material. Metal crystals that appear on the surface of zirconia cause an increase in the intensity of the monoclinic phase of zirconia, supported by its increased degree of crystallinity. Meanwhile, the orthorhombic crystal phase of $Zr(SO_4)_2 \cdot 4H_2O$ disappeared after the impregnation process, which may be because, during the impregnation process, the sulfated zirconia was again immersed in water so that the crystalline salts dissolved and no longer covered the surface of the zirconia.

As shown in Table 1, after treatment with sulfuric acid, zirconia experienced an increase in crystallite size due to the appearance of zirconium sulfate tetrahydrate crystals. After impregnation with nickel and molybdenum metals, the crystallite size of zirconia decreased due to the presence of metal crystals scattered on the surface of zirconia.

3.2 Functional Groups Identification by FTIR

Figure 2 shows the FTIR spectra for zirconia, sulfated zirconia, and NiMo-impregnated sulfated zirconia samples. The absorption peaks at wavenumbers 3426–3449 cm^{-1} indicate the stretching vibrations of the −OH group of water molecules adsorbed on the zirconia surface. In addition, the absorption peak at wavenumbers 1620–1636 cm^{-1}, indicating bending vibrations of the −OH group, also emphasizes this statement [26]. After the sulfation process, the intensity of the peak at the stretching and bending vibrations of the –OH group increased due to the addition of sulfate groups on the zirconia surface, which also brought the appearance of the −OH group from the oxygen atom bound to the sulfur atom. Bending vibrations of the Zr−O−Zr bond framework were observed at wavenumbers 509–741 cm^{-1} [10]. The sharped peak at 1096 cm^{-1} indicates the S−O symmetric vibrations of the bidentate chelation of SO_4^{2-} groups coordinated to Zr^{4+} [27,28]. The dispersion of nickel and molybdenum metals in sulfated zirconia causes a decrease in intensity at these wavenumbers, which supports the XRD results of the

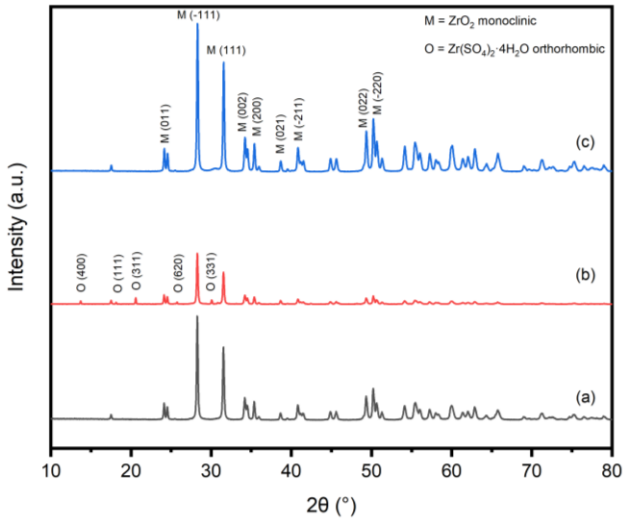

Figure 1. XRD diffractograms of (a) ZrO_2, (b) SO_4–ZrO_2, and (c) NiMo/SO_4–ZrO_2.

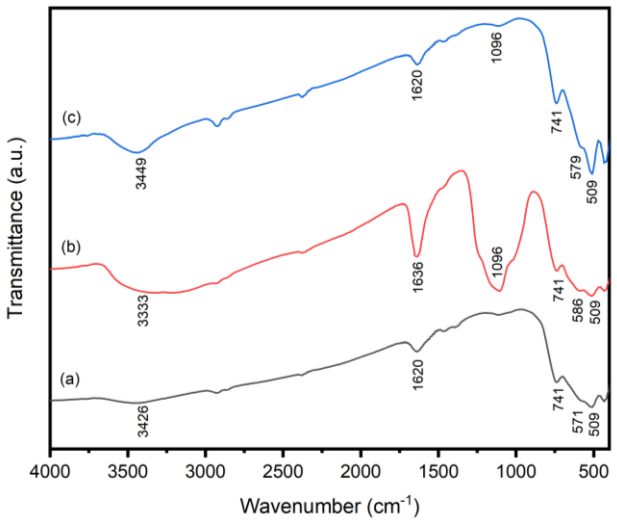

Figure 2. FTIR spectra of (a) ZrO_2, (b) SO_4–ZrO_2, and (c) NiMo/SO_4–ZrO_2.

Table 1. Degree of crystallinity and crystallite size of the catalysts.

Catalyst	Degree of crystallinity (%)	Crystallite size (nm)
ZrO_2	87.0	75.7
SO_4–ZrO_2	85.0	80.0
NiMo/SO_4–ZrO_2	88.0	75.1

disappearance of sulfate salt crystals covering the zirconia surface.

3.3 Total and Surface Acidity Analysis

Figure 3 displays the NH_3-TPD curves for all catalyst samples. The ammonia desorption curves can be divided into two regions: the temperature range of 100–350 °C indicates weak acid sites, while the temperature range of 350–700 °C indicates strong acid sites. Table 2 shows the total acidity values for each catalyst sample.

Zirconia has an acidity value without treatment due to Brønsted acid sites from −OH groups and Lewis acid sites from Zr^{4+} cations [11,29]. After zirconia is treated with sulfuric acid, the total acidity value increases, characterized by the rise in the area of the desorption curve in the strong acid site temperature range. This is because the sulfate group that coats the zirconia material creates new Brønsted acid sites. Meanwhile, after nickel and molybdenum metals were dispersed on sulfated zirconia, the $NiMo/SO_4–ZrO_2$ sample's total acidity value became lower than that of pure zirconia. This phenomenon may be due to the formation of stable zero-valence metal particles covering the surface of sulfated zirconia so that the existence of Brønsted acid sites that initially dominated is blocked.

Testing the acidity value of the catalyst material was also carried out by flowing pyridine vapor under vacuum conditions to the sample. The amount of pyridine successfully adsorbed per gram of sample was represented as the surface acidity value, and the results can be seen in Table 2. A similar trend is also found in the surface acidity value. Sulfated zirconia material has the highest surface acidity value, followed by pure zirconia, and the lowest is NiMo-impregnated sulfated zirconia.

3.4 Textural Properties Analysis

The study of textural properties was carried out using the SAA instrument. The adsorption-desorption isotherm curves of all catalyst samples are presented in Figure 4. All catalyst materials have type IV adsorption-desorption isotherm curves that characterize mesoporous materials. All three samples exhibit H3-type loop hysteresis in which particles aggregate to form slit-shaped pores with narrow edges [21,30]. The amount of N_2 adsorbed by the zirconia material decreased after the sulfation process. However, after the addition of nickel and molybdenum metals, it can be seen that the amount of N_2 adsorbed is much more than before.

The specific surface area, total pore volume, and average pore diameter data of all catalyst materials in Table 3 can explain this phenomenon. Adding sulfuric acid to zirconia material causes a decrease in specific surface area and average pore diameter. We can conclude that this phenomenon occurred due to the pore closure on zirconia by the zirconium sulfate tetrahydrate salt crystals. In

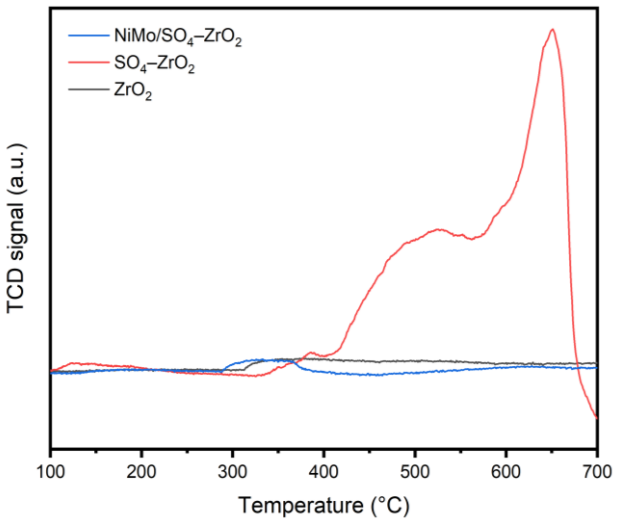

Figure 3. NH_3-TPD profiles of the catalysts.

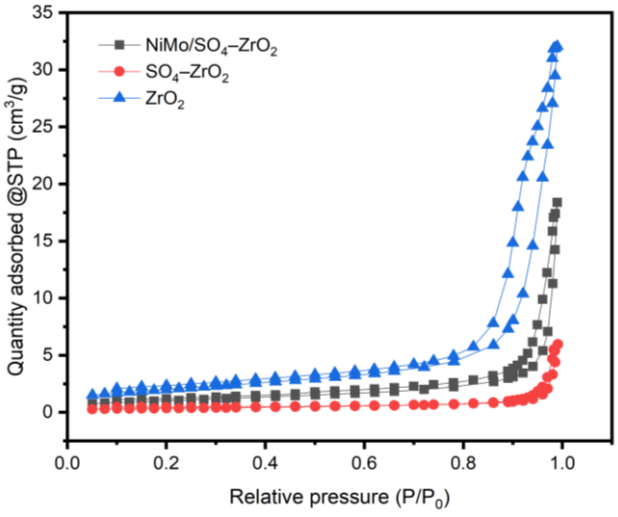

Figure 4. N_2 adsorption-desorption isotherm profiles of the catalysts.

Table 2. Total and surface acidity of the catalysts.

Catalyst	Total acidity (mmol/g NH_3)	Surface acidity (mmol/g C_5H_5N)
ZrO_2	0.130	0.600
$SO_4–ZrO_2$	1.387	1.608
NiMo/ $SO_4–ZrO_2$	0.095	0.397

addition, another study reported that the decrease in specific surface area and average pore diameter is due to the agglomeration of zirconia particles due to their interaction with sulfate groups [27,31]. The increase in crystallite size also supports this statement. However, the sulfation process successfully led to the opening of new pores in the zirconia material, characterized by an increase in total pore volume. Meanwhile, the addition of nickel and molybdenum metals led to an increase in surface area and average pore diameter and a decrease in the total pore volume of sulfated zirconia, which aligns with previous studies [21].

3.5 SEM-EDX Analysis

SEM-EDX images of zirconia, sulfated zirconia, and NiMo/sulfated zirconia catalysts can be seen in Figure 5. All catalyst samples show morphology with grainy, irregular aggregated particles. Zirconia is a crystalline particle with a non-uniform size. After the addition of sulfuric acid, it can be seen that the zirconia particles agglomerate to show a larger particle size [32]. In addition, the surface of sulfated zirconia looks cleaner, which confirms the coating of sulfate groups. Impregnation of nickel and molybdenum metals on sulfated zirconia reduces particle agglomeration and forms new gaps between particles, which can increase specific surface area.

The elemental content on the surface of the catalyst material was determined using EDX, and the results are listed in Table 4. In this study, zirconia nano-powder with high purity was used so that only Zr and O elements were detected. After modification with sulfuric acid, the S

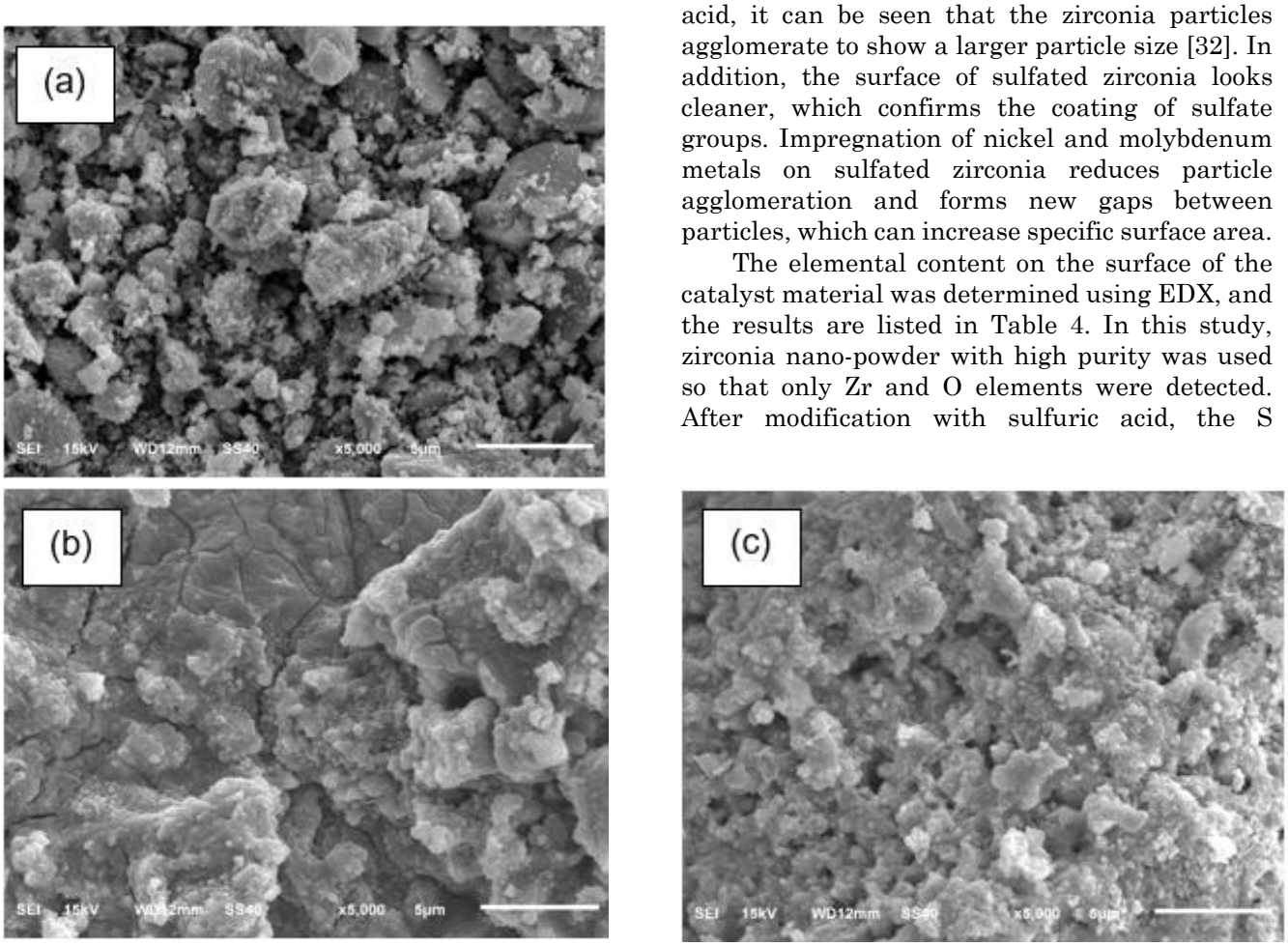

Figure 5. SEM images of (a) ZrO_2, (b) SO_4–ZrO_2, and (c) NiMo/SO_4–ZrO_2 with 5,000 times magnification.

Table 3. Textural properties of the catalysts.

Catalyst	Specific surface area (m^2/g)	Total pore volume (cm^3/g)	Average pore diameter (nm)
ZrO_2	3.58	0.0028	3.78
SO_4–ZrO_2	1.22	0.0088	3.65
NiMo/SO_4–ZrO_2	7.02	0.0050	4.71

Table 4. Elemental composition of the catalysts obtained by EDX.

Catalyst	Element content (wt%)				
	Zr	O	S	Ni	Mo
ZrO_2	73.04	26.96	nd	nd	nd
SO_4–ZrO_2	55.41	38.84	5.75	nd	nd
NiMo/SO_4–ZrO_2	68.29	29.01	0.89	1.03	0.78

nd = not detected

element appeared at 5.75% and decreased after NiMo bimetal impregnation due to the redissolution of $Zr(SO_4)_2 \cdot 4H_2O$ salt. The concentration of each metal impregnated in this study was 1%, and the EDX results showed the percentage of Ni and Mo elements detected were 1.03% and 0.78%, respectively. It can be concluded that the hydrothermal method successfully formed an even metal dispersed on sulfated zirconia as a support material.

3.6 Hydroconversion of Used Palm Cooking Oil using the Catalysts Evaluation

In this study, the hydroconversion process was carried out using atmospheric pressure to meet green chemistry principles better because high hydrogen gas pressure is too dangerous. Table 5 presents the total conversion results of used palm cooking oil into liquid, coke, and gas products, where the amount of liquid products produced represents the catalyst activity. The residue is defined as the unreacted feed left in the reactor.

Zirconia catalyst can transform used palm cooking oil into liquid products only 40.73%. The modification with sulfuric acid and continued with NiMo bimetal impregnation increased the liquid product produced by 51.53% and 61.07%, respectively. Sulfated zirconia catalyst has better activity than zirconia, supported by an increase in acidity both total and surface, which the more acid sites on a catalyst material used in the hydroconversion process, the more carbonium ions will be formed as a starting point of the hydrocracking reaction so that more hydrocarbon compounds will be produced. However, sulfated zirconia has a worse specific surface area and average pore diameter than zirconia, so more than acidity is needed to guarantee that a catalyst will perform better in hydroconversion. A high acidity value can also cause the catalyst to deactivate quickly, supported by the high coke percentage (0.68%).

On the other hand, sulfated zirconia impregnated with nickel and molybdenum successfully showed superior catalytic activity because this material has a better specific surface area and average pore diameter compared to sulfated zirconia so that feed molecules in the form of triglycerides or free fatty acids can more easily access the active sites of the catalyst. Therefore, the hydroconversion process becomes more optimal. Using NiMo-impregnated sulfated zirconia catalyst can also suppress the formation of coke and gas products. Xu *et al.* [33] reported that the relationship between a catalyst's pore size, acidity, and impregnated metal content must be considered to lessen the likelihood of catalyst active site deactivation.

GC-MS analysis of the liquid product was carried out to study catalyst selectivity in the formation of bio-hydrocarbon fractions that compose jet fuel (C_8–C_{16}). Four groups of compounds are present in the liquid product from the hydroconversion of used palm cooking oil, including biogasoline (C_5–C_7), bio-jet fuel (C_8–C_{16}), biodiesel (>C_{16}), and non-hydrocarbons. The selectivity for each catalyst has been summarized in Table 6.

Zirconia catalyst has the lowest selectivity to bio-jet fuel, followed by sulfated zirconia, and the best is NiMo-impregnated sulfated zirconia. In the use of sulfated zirconia catalyst, a certain amount of bio-hydrocarbons in the gasoline range was

Table 5. The catalytic activity of the catalysts toward hydroconversion of used palm cooking oil.

Catalyst	Yield (wt%)			Residue (wt%)	Total conversion (wt%)
	Liquid	Coke	Gas		
ZrO_2	40.73	0.56	58.71	23.33	76.67
SO_4–ZrO_2	51.53	0.61	47.86	23.33	76.67
NiMo/SO_4–ZrO_2 (fresh)	61.07	0.28	38.65	16.67	83.33
NiMo/SO_4–ZrO_2 (1st reuse)	63.67	0.30	36.03	16.67	83.33
NiMo/SO_4–ZrO_2 (2nd reuse)	62.47	0.72	36.81	16.67	83.33

Table 6. The selectivity of the catalysts toward the liquid product from hydroconversion of used palm cooking oil.

Catalyst	Selectivity (wt%)			
	Bio-jet fuel	Biogasoline	Biodiesel	Non-hydrocarbon
ZrO_2	27.76	0.00	7.88	5.09
SO_4–ZrO_2	34.34	0.66	10.17	3.36
NiMo/SO_4–ZrO_2 (fresh)	43.49	0.00	14.42	3.16
NiMo/SO_4–ZrO_2 (1st reuse)	51.68	0.46	4.99	6.53
NiMo/SO_4–ZrO_2 (2nd reuse)	30.86	0.00	12.99	18.61

found (0.66%), which means that the too-high acidity value of the catalyst causes the hydrocracking reaction to excessively produce short-chain hydrocarbons. Of the three catalysts tested, the NiMo/SO_4–ZrO_2 catalyst showed the lowest percentage of non-hydrocarbon compounds (free fatty acid, aldehyde, or ketone). This indicates a synergistic effect between nickel and molybdenum metals in hydrodeoxygenation and hydrocracking reactions.

For comparison, the jet fuel fraction (C_8–C_{16}) of the liquid hydroconversion product using fresh NiMo/SO_4–ZrO_2 catalyst was compared with the commercial jet fuel sample to determine the composition of each constituent hydrocarbon (Figure 6). Commercial jet fuel is dominated by C_{10} and C_{12} hydrocarbons, while our bio-jet fuel has dominant hydrocarbons in C_{14} and C_{16}. These results indicate that there is still a need for further optimization of the hydroconversion process, such as examining the catalyst-to-feed ratio, reaction time, reaction temperature, and hydrogen gas flow rate so that the hydrodeoxygenation and hydrocracking reactions can run more optimally and, therefore, produce better bio-jet fuel selectivity.

The reusability test was also conducted on the NiMo/SO_4–ZrO_2 catalyst for three consecutive runs. Overall, this catalyst still performs well when used for three cycles. Based on the data in Table 5, the hydroconversion process with the second use of NiMo/SO_4–ZrO_2 catalyst successfully increased the amount of liquid product formed. This can be caused by the catalyst experiencing self-activation due to the heating treatment after the first use. Activation due to thermal treatment is possible to open the pores and prepare the catalyst for adsorbing feed molecules. It is also consistent with the data in Table 6 that the selectivity of bio-jet fuel produced in the second run is higher than in the first run. In the third run, the catalyst began to experience a decrease in both liquid product and bio-jet fuel selectivity. This can be explained by the buildup of coke covering the active sites of the catalyst so that the feed becomes challenging to crack into hydrocarbon compounds [34]. SEM-EDX analysis of the spent NiMo/SO_4–ZrO_2 catalyst after three consecutive runs was conducted to corroborate this statement.

Figure 7 shows that the spent NiMo/SO_4–ZrO_2 catalyst has a morphology that is not too different from fresh NiMo/SO_4–ZrO_2. At some points, the morphology of the catalyst particles becomes darker, indicating coke deposits on the surface. This is confirmed by the EDX results in Table 7, showing that 29.90% of carbon element was detected in the spent NiMo/SO_4–ZrO_2 catalyst. In addition, sulfur and molybdenum elements were also not detected, which reinforces the presence of coke covering the active sites of the catalyst, decreasing its catalytic performance.

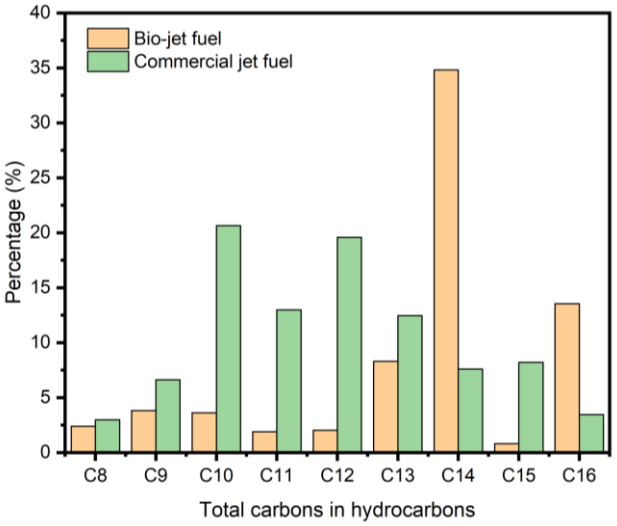

Figure 6. Diagram of hydrocarbon distribution comparison in bio-jet fuel and commercial jet fuel.

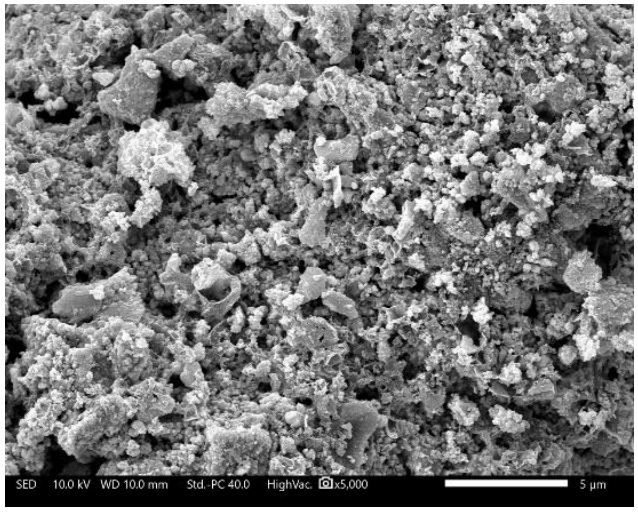

Figure 7. SEM image of the spent NiMo/SO_4–ZrO_2 after three runs hydroconversion process with 5,000 times magnification.

Table 7. Elemental composition of the spent NiMo/SO_4–ZrO_2 catalyst after three runs hydroconversion process obtained by EDX.

Element content (wt%)					
Zr	O	S	Ni	Mo	C
51.10	18.72	nd	0.28	nd	29.90

nd = not detected

Table 8 summarizes previous research results on bio-jet fuel production using different feeds, catalysts, process conditions, and reactor types. The hydroconversion process using atmospheric pressure is promising regarding the bio-jet fuel produced, which is much safer than high-pressure hydroconversion. Our catalyst NiMo/SO_4–ZrO_2 is also superior to others; thus, the surface modification of zirconia with sulfuric acid coupled with nickel-molybdenum bimetal impregnation has created a catalyst system that synergizes with each other in catalyzing the transformation of feed into bio-jet fuel. Then, we can also conclude that used palm cooking oil, which is vegetable waste, has the potential to be used as feed in bio-jet fuel production. This conversion step is also a form of overcoming waste contamination to achieve sustainable development goals.

4. Conclusion

Modifying commercial nano-zirconia powder with sulfuric acid proceeded by impregnation of nickel and molybdenum bimetal via hydrothermal method has been successfully carried out. The sulfation process successfully increased zirconia's total and surface acidity values but decreased the specific surface area and average pore diameter. Meanwhile, NiMo bimetal impregnation successfully increased the specific surface area and pore diameter, although the catalyst is minor in acidity. NiMo/SO_4–ZrO_2 showed the best catalytic performance for bio-jet fuel production from used palm cooking oil with liquid products and selectivity of 61.07% and 43.49%, respectively. This catalyst has relatively good stability after being used for three consecutive runs. Further research is needed to determine the best process conditions, such as catalyst-to-feed ratio, reaction time, reaction temperature, and hydrogen gas flow rate. Therefore, maximum bio-jet fuel fractions will be obtained.

Acknowledgments

This research was fully supported by the facilities of the Physical Chemistry Laboratory, Department of Chemistry, Universitas Gadjah Mada, and Advanced Characterization Laboratories Serpong, the National Research and Innovation Agency (BRIN) Indonesia.

CRediT Author Statement

Author Contributions: *K. Wijaya*: Conceptualization, Project Administration, Resources, Data Curation, Writing, Review and Editing, Supervision, Validation; *A. J. Saviola*: Conceptualization, Methodology, Investigation, Formal Analysis, Data Curation, Writing Draft Preparation, Visualization, Software, Validation; *A. K. Amin*: Validation, Writing, Review and

Table 8. Summary of bio-jet fuel production comparison with some previous studies.

Feed	Catalyst	Process conditions	Reactor type	Liquid product (wt%)	Bio-jet fuel selectivity (wt%)	Ref.
Used palm cooking oil	NiMo/SO_4–ZrO_2	300–600 °C, 1 atm, 2 h	Semi-batch with a double furnace reactor	61.07	43.49	This work
Used palm cooking oil	NiMo-2/SiO_2	425 °C, 1 atm, 2 h	Multilevel reactor	42.80	39.48	[4]
Used palm cooking oil	PO_4–ZrO_2	550 °C, 1 atm, 2 h	Semi-batch with a double furnace reactor	39.44	33.92	[24]
Refined palm kernel oil	15-Mo/Mor	300–600 °C, 1 atm, 4 h	Semi-batch with a double furnace reactor	46.08	43.19	[35]
Jatropha oil	4% MB	300–450 °C, 78.95 atm, 18 min	Stainless-steel bench scale high pressure and temperature-batch reactor	ns	40.00	[36]
Crude palm kernel oil	Pt/C	420 °C, 34 atm, 1 h	Fixed bed reactor	91.44	58.29	[37]

ns = not stated

Editing, Data Curation; *M. F. Vebryana*: Methodology, Investigation, Writing, Review and Editing. *A. Bhagaskara*: Methodology, Investigation, Writing, Review and Editing, Visualization, Software. *H. A. Ekawati*: Methodology, Investigation, Writing, Review and Editing. *S. Ramadhani*: Methodology, Investigation, Writing, Review and Editing. *D. A. Saputra*: Validation, Writing, Review and Editing, Data Curation. *A. Agustanhakri*: Validation, Writing, Review and Editing, Data Curation. All authors have read and agreed to the published version of the manuscript.

References

[1] Fan, Y.V., Perry, S., Klemeš, J.J., Lee, C.T. (2018). A review on air emissions assessment: Transportation. *Journal of Cleaner Production*, 194, 673–684. DOI: 10.1016/j.jclepro.2018.05.151.

[2] El-Araby, R., Abdelkader, E., El Diwani, G., Hawash, S.I. (2020). Bio-aviation fuel via catalytic hydrocracking of waste cooking oils. *Bulletin of the National Research Centre*, 44, 1–9. DOI: 10.1186/s42269-020-00425-6.

[3] Doliente S.S, Narayan A, Tapia JFD, Samsatli N.J., Zhao Y, Samsatli S (2020). Bio-aviation Fuel: A Comprehensive Review and Analysis of the Supply Chain Components. *Frontiers in Energy Research,* 8, 1–38. DOI: 10.3389/fenrg.2020.00110.

[4] Agharadatu, R.H., Wijaya, K., Prastyo, Wangsa, Hauli, L., Oh, W.-C. (2024). Application of Mesoporous NiMo/Silica (NiMo/SiO_2) as a Catalyst in the Hydrocracking of Used Cooking Oil into Jet Fuel. *Silicon*, 16, 331–343. DOI 10.1007/s12633-023-02683-1.

[5] Foo, W.H., Chia, W.Y., Tang, D.Y.Y., Koay, S.S.N., Lim, S.S. Chew, K.W. (2021) The conundrum of waste cooking oil: transforming hazard into energy. *Journal of Hazardous Materials*, 417, 126129. DOI: 10.1016/j.jhazmat.2021.126129.

[6] Zhang, Z., Wang, Q., Chen, H., Zhang, X. (2017). Hydroconversion of Waste Cooking Oil into Green Biofuel over Hierarchical USY-Supported NiMo Catalyst: A Comparative Study of Desilication and Dealumination. *Catalysts,* 7, 281. DOI: 10.3390/CATAL7100281.

[7] Lin, C.H., Chen, Y.K., Wang, W.C. (2020). The production of bio-jet fuel from palm oil derived alkanes. *Fuel*, 260, 116345. DOI: 10.1016/j.fuel.2019.116345.

[8] Dobrosz-Gómez, I., Gómez-García, M.Á., Bojarska, J., Kozanecki, M., Rynkowski, J.M. (2015). Combustion synthesis and properties of nanocrystalline zirconium oxide. *Comptes Rendus Chimie*, 18, 1094–1105. DOI: 10.1016/j.crci.2015.02.007.

[9] Suseno, A., Wijaya, K., Trisunaryanti, W., Shidiq, M. (2015). Synthesis and Characterization of ZrO_2-Pillared Bentonites. *Asian Journal of Chemistry*, 27, 2619–2623. DOI: 10.14233/ajchem.2015.18599.

[10] Amin, A.K., Wijaya, K., Trisunaryanti, W. (2020). Physico-Chemical Properties of Nickel Promoted Sulfated Zirconia Powder Prepared using Different Procedures. *Asian Journal of Chemistry*, 32, 555–560. DOI: 10.14233/ajchem.2020.21991.

[11] Wijaya, K., Utami, M., Damayanti, A.K., Tahir, I., Tikoalu, A.D., Rajagopal, R., Thirupathi, A., Ali, D., Alarifi, S., Chang, S.W., Ravindran, B. (2022). Nickel-modified sulfated zirconia catalyst: synthesis and application for transforming waste cooking oil into biogasoline via a hydrocracking process. *Fuel*, 322, 124152. DOI: 10.1016/j.fuel.2022.124152.

[12] Meng, S., Li, W., Li, Z., Song, H., (2023). Recent progress of the transition metal-based catalysts in the catalytic biomass gasification: A mini-review. *Fuel*, 353, 129169. DOI: 10.1016/j.fuel.2023.129169.

[13] Chen, W., Wu, Z., Peng, R., Wu, W., Li, X., Cao, D., Zhang, Z., Niu, K. (2023). Low-cost diatomite supported binary transition metal sulfates: an efficient reusable solid catalyst for biodiesel synthesis. *RSC Advances*, 13, 6002–6009. DOI: 10.1039/D2RA07947J.

[14] Al-Marshed, A., Hart, A., Leeke, G., Greaves, M. Wood, J. (2015). Effectiveness of different transition metal dispersed catalysts for in situ heavy oil upgrading. *Industrial & Engineering Chemistry Research*, 54, 10645–10655. DOI: 10.1021/acs.iecr.5b02953.

[15] Chintakanan, P., Vitidsant, T., Reubroycharoen, P., Kuchonthara, P., Kida, T., Hinchiranan, N. (2021). Bio-jet fuel range in biofuels derived from hydroconversion of palm olein over Ni/zeolite catalysts and freezing point of biofuels/Jet A-1 blends. *Fuel*, 293, 120472. DOI: 10.1016/j.fuel.2021.120472.

[16] Kaewtrakulchai, N., Smuthkochorn, A., Manatura, K., Panomsuwan, G., Fuji, M., Eiad-Ua, A. (2022). Porous Biochar Supported Transition Metal Phosphide Catalysts for Hydrocracking of Palm Oil to Bio-Jet Fuel. *Materials*, 15, 6584. DOI: 10.3390/ma15196584.

[17] Imai, H., Kimura, T., Terasaka, K., Li, X., Sakashita, K., Asaoka, S., Al-Khattaf, S.S. (2018). Hydroconversion of fatty acid derivative over supported Ni-Mo catalysts under low hydrogen pressure. *Catalysis Today*, 303, 185–190. DOI: 10.1016/j.cattod.2017.08.023.

[18] Wang, J., Mo, F., Fei, J., Ling, W., Cui, M., Lei, H., Jiang, L., Huang, Y., (2022). Insights into the synergistic effect between nickel and molybdenum for catalyzing urea electrooxidation. *Carbon Neutralization*, 1, 267–276. DOI: 10.1002/cnl2.27

[19] Lin, C.H., Chen, Y.K., Wang, W.C. (2020). The production of bio-jet fuel from palm oil derived alkanes. *Fuel*, 260, 116345. DOI: 10.1016/j.fuel.2019.116345.

[20] Cai, Z., Ding, Y., Zhang, J., Yu, P., Ma, Y., Cao, Y., Zheng, Y., Huang, K., Jiang, L. (2023). In situ generation of dispersed MoS2 catalysts from oil-soluble Mo-based ionic liquids for highly effective biolipids hydrodeoxygenation. *Journal of Catalysis*, 423, 50–61. DOI: 10.1016/j.jcat.2023.04.022.

[21] Hanifa, A., Nadia, A., Saputri, W.D., Syoufian, A., Wijaya, K. (2021). Performance of Ni-Mo Sulfated Nanozirconia Catalyst for Conversion of Waste Cooking Oil into Biofuel via Hydrocracking Process. *Materials Science Forum*, 1045, 79–89. DOI: 10.4028/www.scientific.net/MSF.1045.79.

[22] Huerta-Mata, C.A., Chowdari, R.K., Soto-Arteaga, C.E., Infantes-Molina, A., Alonso-Núnez, G., Fuentes-Moyado, S., Huirache-Acuña, R., Díaz de León, J.N. (2022). Hydrothermal synthesis of bulk Ni impregnated WO_3 2D layered structures as catalysts for the desulfurization of 3-methyl thiophene. *Chemical Engineering Journal Advances*, 11, 100312. DOI: 10.1016/j.ceja.2022.100312.

[23] Feng, S., Li, G. (2017). Hydrothermal and solvothermal syntheses. *Modern Inorganic Synthesis Chemistry (Second Edition)*. 73–104. DOI: 10.1016/B978-0-444-63591-4.00004-5.

[24] Saviola, A.J., Wijaya, K., Syoufian, A., Saputri, W.D., Saputra, D.A., Aziz, I.T.A., Oh, W.-C. (2024). Hydroconversion of used palm cooking oil into bio-jet fuel over phosphoric acid-modified nano-zirconia catalyst. *Case Studies in Chemical and Environmental Engineering*, 9, 100653. DOI: 10.1016/j.cscee.2024.100653.

[25] Yu, P., Chen, C., Li, G., Wang, Z., Li, X. (2020). Active, Selective, and Recyclable $Zr(SO_4)_2/SiO_2$ and $Zr(SO_4)_2$/Activated Carbon Solid Acid Catalysts for Esterification of Malic Acid to Dimethyl Malate. *Catalysts*, 10, 384. DOI: 10.3390/catal10040384.

[26] Utami, M., Wijaya, K. Trisunaryanti, W. (2017). Effect of sulfuric acid treatment and calcination on commercial zirconia nanopowder. *Key Engineering Materials*, 757, 131–137. DOI: 10.4028/www.scientific.net/KEM.757.131.

[27] Utami, M., Trisunaryanti, W. Shida, K., Tsuhida, M., Kawakita, H., Ohto, Wijaya, K., Tominaga, M. (2019). Hydrothermal preparation of a platinum-loaded sulphated nanozirconia catalyst for the effective conversion of waste low density polyethylene into gasoline range hydrocarbons. *RSC Advances*, 9, 41392–41401. DOI: 10.1039/C9RA08834B.

[28] Sekawael, S.J., Pratika, R.A., Hauli, L., Amin, A.K., Utami, M., Wijaya, K. (2022). Recent Progress on Sulfated Nanozirconia as a Solid Acid Catalyst in the Hydrocracking Reaction. *Catalysts*, 12, 191. DOI: 10.3390/catal12020191.

[29] La Ore, M.S., Wijaya, K., Trisunaryanti, W., Saputri, W.D., Heraldy, E., Yuwana, N.W., Hariani, P.L., Budiman, A., Sudiono, S. (2020). The synthesis of SO_4/ZrO_2 and Zr/CaO catalysts via hydrothermal treatment and their application for conversion of lowgrade coconut oil into biodiesel. *Journal of Environmental Chemical Engineering*, 8, 104205. DOI: 10.1016/j.jece.2020.104205.

[30] Thommes, M., Kaneko, K., Neimark, A.V., Olivier, J.P., Rodriguez-reinoso, F., Rouquerol, J., Sing, K.S.W. (2015). Physisorption of gases, with special reference to the evaluation of surface area and pore size distribution (IUPAC Technical Report). *Pure and Applied Chemistry*, 87, 1051–1069. DOI: 10.1515/pac-2014-1117.

[31] Utami, M., Wijaya, K., Trisunaryanti, W. (2018). Pt-promoted sulfated zirconia as catalyst for hydrocracking of LDPE plastic waste into liquid fuels. *Materials Chemistry and Physics*, 213, 548–555. DOI: 10.1016/j.matchemphys.2018.03.055.

[32] Hauli, L., Wijaya, K., Syoufian, A. (2019) Hydrocracking of LDPE plastic waste into liquid fuel over sulfated zirconia from a commercial zirconia nanopowder, *Oriental Journal of Chemistry*, 35, 128–133, DOI: 10.13005/ojc/350113.

[33] Xu, Y., Du, X.H., Li, J., Wang, P., Zhu, J. Ge, F.J., Zhou, J., Song, M., Zhu, W.Y. (2019) A comparison of Al_2O_3 and SiO_2 supported Ni-based catalysts in their performance for the dry reforming of methane. *Journal of Fuel Chemistry and Technology*, 47, 199–208. DOI: 10.1016/S1872-5813(19)30010-6.

[34] Ibrahim, M.S., Trisunaryanti, W., Triyono T. (2022) Nickel supported parangtritis beach sand (PP) catalyst for hydrocracking of palm and Malapari oil into biofuel. *Bulletin of Chemical Reaction Engineering and Catalysis*, 17, 638–649. DOI: 10.9767/bcrec.17.3.15668.638-649.

[35] Trisunaryanti, W., Wijaya, K., Triyono, Kartini, I., Rodiansono, Purwono, S., Mara, A., Budiansyah, A. (2023). Preparation of Mo-impregnated mordenite catalysts for the conversion of refined kernel palm oil into bioavtur, *Communications in Science and Technology*, 8, 226–234, DOI: 10.21924/cst.8.2.2023.1288.

[36] Hasan, S.H., Attia, N.K., El Diwani, G.I., Amin, S.K.M Ettouney, R.S. El-Rifai M.A. (2023). Catalytic hydrocracking of jatropha oil over natural clay for bio-jet fuel production. *Scientific Reports*, 13, 13419. DOI: 10.21203/rs.3.rs-2956399/v1.

[37] Makcharoen, M., Kaewchada, A., Akkarawatkhoosith, N. (2021). Biojet fuel production via deoxygenation of crude palm kernel oil using Pt/C as catalyst in a continuous fixed bed reactor. *Energy Conversion and Management: X*, 12, 100125. DOI: 10.1016/j.ecmx.2021.100125.